Active Saffman-Taylor Viscous Fingering

Akash Ganesh, Carine Douarche, Harold Auradou

Active Saffman–Taylor Viscous Fingering

Akash Ganesh, Carine Douarche, and Harold Auradou*
Université Paris-Saclay, CNRS, FAST, 91405, Orsay, France.

Adding swimming bacteria to a liquid causes its effective shear viscosity to decrease, eventually reaching a regime of zero viscosity. We examined whether this property leads to viscous finger-like displacement fronts like those observed when a less viscous fluid displaces a more viscous liquid. Our study revealed that this system exhibits more complex dynamic characteristics than the classical Saffman–Taylor instability. We discovered that this instability occurs when the bacterial volume fraction exceeds a critical value, and the imposed shear rate is below critical value, for which the viscosity of the suspension is zero.

Introduction.- An individual bacterium has the ability to convert the chemical energy present in the surrounding fluid into mechanical motion (swimming) [1, 2]. From the swimming of a population of bacteria, emerge at large scales, interesting properties of the fluid, such as the appearance of coherent dynamic structures [3–6], unidirectional flows [7, 8], enhanced dispersion [9–12], active motion of small objects [13–15], dynamical clustering of passive particles [17] *etc.* Such properties have made bacterial suspensions a popular model system for exploring the physical properties of active fluids [18–20]. One of the interesting properties observed in a suspension of bacteria is their ability to reduce the effective viscosity of the suspension when it is subject to a moderate shear [21–32]. This emergence is due to the fact that the spatially organized stress response generated by the bacteria motion aids the applied shear stress, leading to a decrease in the effective viscosity [26, 30]. The effective viscosity of the bacterial suspension decreases linearly when increasing the volume fraction ϕ_0 of bacteria [21–23, 30] until a critical bacterial volume fraction ϕ_c is reached. Above this concentration, the activity of the bacteria is such that the viscosity becomes zero [21–23]. Our study demonstrates that the viscosity reduction observed when bacteria are added in a fluid can influence macroscopic flows and leads to flow instability such as Saffman–Taylor instability (also known as viscous fingering) observed when a less viscous fluid displaces a more viscous fluid [33–46]. To demonstrate how the flow of bacterial suspensions can cause instabilities, we conducted experiments using the Saffman–Taylor geometry, which involves a Hele-Shaw (HS) cell with parallel plates separated by a small aperture H. We identified the bacterial volume fraction and flow rate at which these instabilities occur. Additionally, we performed experiments in the quarter five-spot (QFS) configuration [44, 46] to confirm the occurrence of multiple unstable fingers. These experiments also confirmed the significant role of the critical volume fraction ϕ_c coupled with a critical shear rate $\dot{\gamma}_c$ in triggering the instability.

Methods.- We used a wild-type strain of *Escherichia coli* (*E. coli*) (RP437-YFP) that expresses

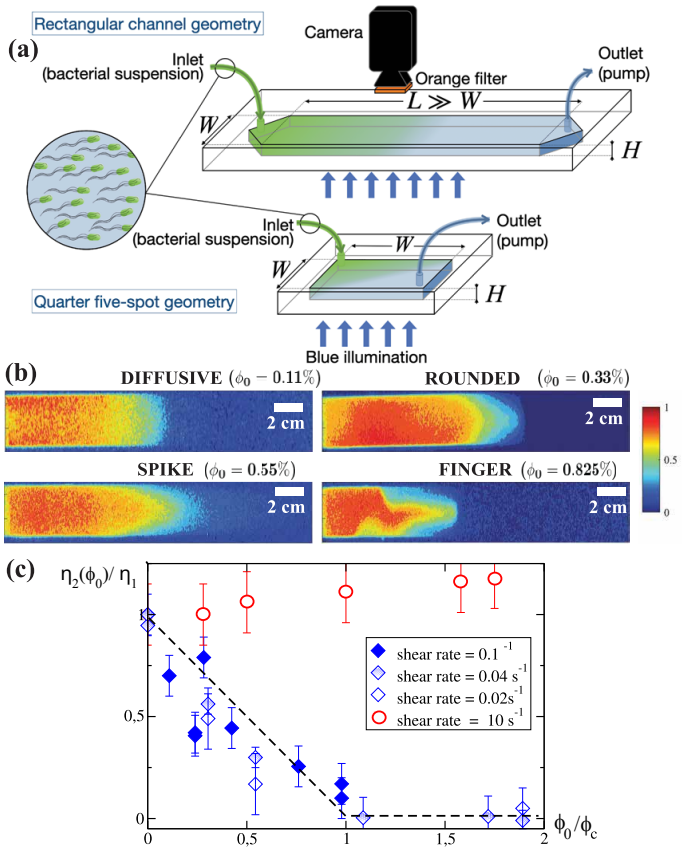

FIG. 1. (a) Schematic representations of the HS and QFS geometries. Fluorescent bacteria are injected into the aperture initially filled with a buffer and visualized with a camera through a colored filter. HS cells measure $L = 21$ cm in length, $W = 1$ or 2 cm in width, and $H = 500$ μm in aperture (top panel). QFS devices are squares with sides 5 cm and $H = 500$ μm aperture (down panel). (b) Fronts observed for four different bacterial volume fractions ϕ_0. (c) Viscosities of the bacterial suspensions measured in a Couette rheometer [21–23] at shear rates lower (◊) and higher (◯) than the critical shear rate $\dot{\gamma}_c = 0.4$ s^{-1} as function of ϕ_0. Dashed line: a visual guide for viscosity measurements using the mean-field continuum kinetic theory model [22, 26].

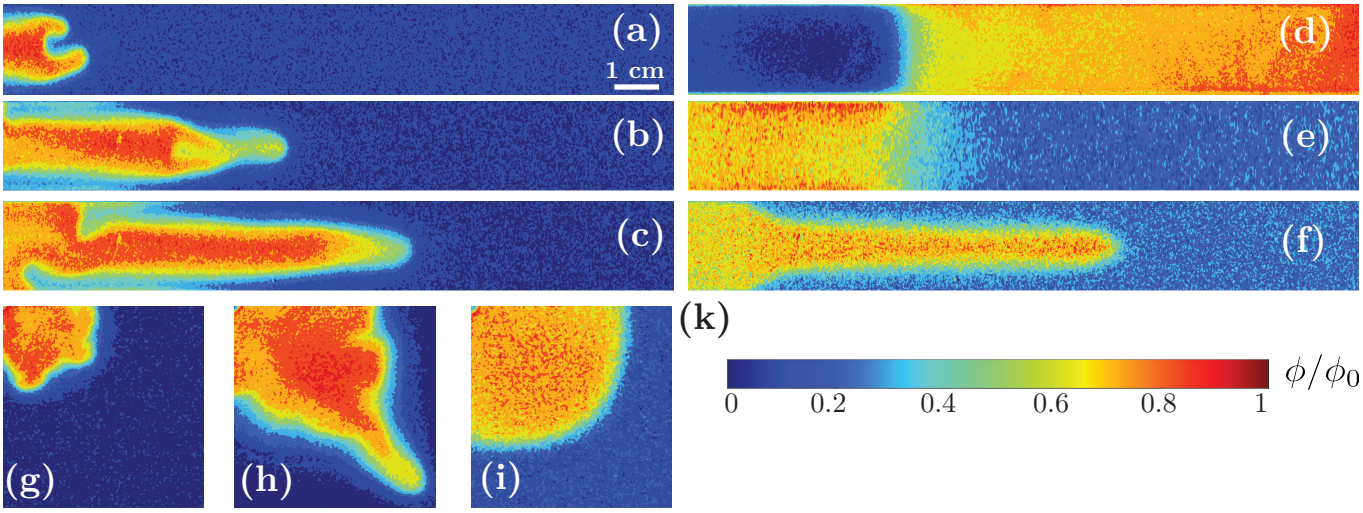

FIG. 2. (a)-(c) Normalized bacterial volume fraction fields $\phi(x,y)/\phi_0$ for an experiment in HS cell of width $W = 2$ cm. The volume fraction of bacteria in the injected fluid is $\phi_0 \approx 0.825\% > \phi_c$. The images are taken 30 min apart. (d) Bacterial suspension of volume fraction $\phi_0 \approx 0.825\%$ displaced by the suspending fluid (reverse of (a)-(c)).(e) $\phi(x,y)/\phi_0$ when $\phi_0 \approx 0.11\% < \phi_c$. (f) Experiment with Newtonian fluids with $M = 6.5$. For (a)-(f): $U \simeq 17$ μm.s^{-1}. (g)-(i) Normalized bacterial volume fraction fields $\phi(x,y)/\phi_0$ for experiments in the QFS geometry at $U \simeq 10$ μm.s^{-1} with (g,h) $\phi_0 \approx 0.825\% > \phi_c$ and (i) $\phi_0 \approx 0.11\% < \phi_c$. (k) Color bar for all the fields. The scale bar for all figures is specified in bottom right of (a).

yellow fluorescence protein. Bacteria were suspended in a motility buffer (MB) containing 1% of PolyVinylPyrolydine (MB-1%PVP) (SI I). The concentration of bacteria is given in terms of volume fraction ϕ, which was estimated from the OD (optical density) of the suspension with 1 OD corresponding to $\sim 8.10^5$ cells/μL. Assuming the volume of an individual bacterium to be ~ 1.4 μm^3 [21], this corresponds to a volume fraction $\phi \sim 0.11\%$. The average swimming velocity (V_s) and the rotational diffusivity (D_R) were obtained by tracking a dilute bacterial suspension under a microscope using a 10× objective (SI II). We observed $V_s = 15.0 \pm 1.2$ μm.s^{-1} and $D_R = 0.09 \pm 0.02$ s^{-1} when bacteria were suspended in MB-1%PVP. The critical volume fraction was determined from rheological measurements conducted in a Couette rheometer [21–23]. ϕ_c was taken between the last volume fraction with non-zero viscosity and the first volume fraction with zero viscosity. This gives $\phi_c = 0.66 \pm 0.05\%$ for bacteria suspended in MB-1%PVP. The rheological measurements (Fig. 1(c)) also confirmed that at a shear rate lower than 0.1 s^{-1}, the viscosity, $\eta_2(\phi_0)$, of the suspension is lower than the viscosity, η_1, of the same fluid without bacteria, confirming the behavior already reported in the literature [21–23].

The flow cells were created by pouring Polydimethylsiloxane (PDMS) onto master molds to produce replicas, which were then bonded to a thick glass plate through plasma activation (Fig. 1(a)). PDMS is highly permeable to dioxygen, preventing the loss of bacterial motility. The outlets were connected to a syringe pump that draws in the bacterial suspension from a reservoir connected to the channel's inlet at a fixed flow rate. The channel was first filled with the suspending fluid ($\eta_1 = 3.2 \pm 0.1$ mPa.s) before the injection of the bacterial suspension. The channels were placed on top of a blue-light illumination table and a 16-bit CCD camera with an orange filter to visualize the progression of the bacterial concentration front. A calibration was performed to convert the fluorescence intensity integrated over the HS cell aperture into local bacterial volume fraction $\phi(x,y,t)$. The experiments were performed at different volume fractions ϕ_0. The average flow velocity of the bacterial front U was determined by performing flow displacement experiments at different flow rates using a dilute suspension $\phi_0 \simeq 0.066\% << \phi_c$ [16]. Fig. 1(b) shows typical fields obtained with a spatial resolution of 500 μm for different bacterial volume fractions.

Results.- The images presented in Fig. 1(b) provide clear evidence of the crucial role of the bacterial concentration in determining the shape of the displacing front. Based on the observations of the shapes, we identified four distinct fronts: diffusive, rounded, spike, and finger. The Fig. 2(a-c) and Movie1 show the typical evolution of the unstable finger-like front. At the early stage of the instability (Fig. 2(a)), the front showed two protrusions that were not present when the suspension contained a lower volume fraction of bacteria (Fig. 2(e)). One of the protrusions expanded slightly ahead of its neighbor (Fig. 2(b)) and led to the emergence of a single finger (Fig. 2(c)). The back of the finger then expanded until it filled the entire width of the channel (Fig. 2(c)). The final finger shape observed in Fig. 2(c), looked similar to the fronts obtained experimentally [34, 43, 45, 47, 48] and

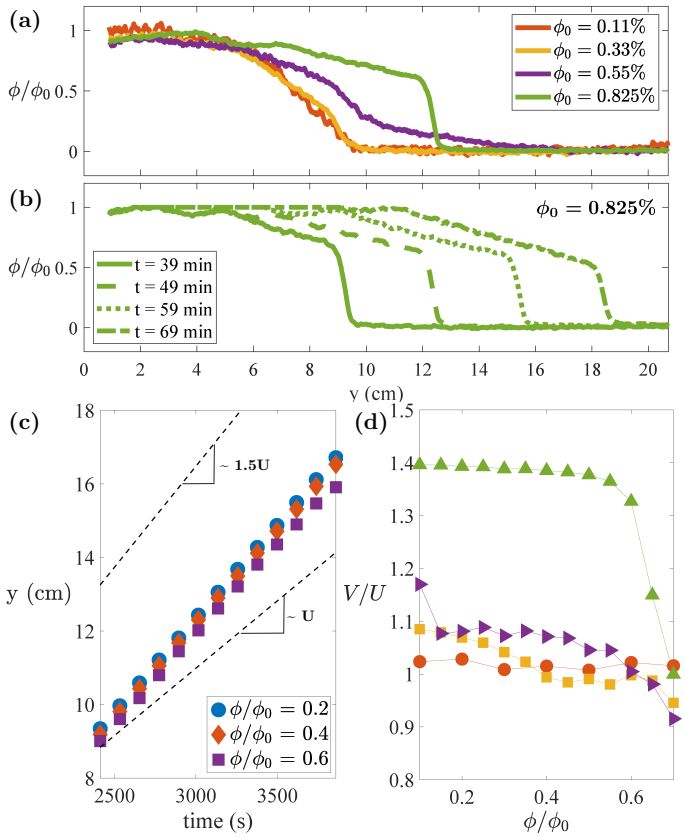

FIG. 3. (a) Bacterial volume fraction profiles measured in an HS cell of width $W = 1$ cm plotted as a function of the distance, y, along the length of the cell. The profiles are obtained by averaging $\phi(x, y)$ in the direction of the cell width over a band of width 5 mm passing through the center of the HS. The profiles are for a fixed time of $\sim$ 50 min and for different volume fractions ϕ_0. (b) Profiles at different time measured for $\phi_0 \approx 0.825\%$ ($> \phi_c$). (c) y position of the concentration profiles shown in (b) for three iso-volume fractions $\phi/\phi_0 = 0.2$ (◯), 0.4 (◇), and 0.6 (□) as a function of time. The slopes of these plots give $V(\phi/\phi_0)$. The dashed lines are a guide for the eyes. Here: $\phi_0 \approx 0.825\%$. (d) $V(\phi/\phi_0)/U$ as a function of ϕ/ϕ_0 for: $\phi_0 \approx 0.11\%(< \phi_c)$ (◯), $\phi_0 \approx 0.33\%(< \phi_c)$ (□), $\phi_0 \approx 0.55\%(< \phi_c)$ (▷) and $\phi_0 \approx 0.825\%(> \phi_c)$ (△). All experiments were done with $U \simeq 37$ μm.s^{-1}.

through simulations [49] with miscible or immiscible pair of Newtonian fluids. This was confirmed by conducting experiments with pairs of Newtonian fluids containing different quantities of PVP, the concentration of which was adjusted so that M, the viscosity ratio between the displaced and the displacing fluids, varied between 1 and 12. In these experiments, bacteria were replaced by fluorescein at a concentration of 0.02 g/L to visualize the progression of that fluid. Fig. 2(f) shows one of the images obtained for $M \simeq 6.5$. The width of finger observed was similar to the one shown in Fig. 2(c). Fig. 2(d) shows an image obtained when the displaced and displacing fluids were swapped in the bacteria experiment ($\phi_0 > \phi_c$ here as well). Under this condition, the interface was stable, and no finger was observed (Movie2). To confirm the role of the swimming activity of bacteria in the formation of the finger, and to eliminate the possibility of hydrodynamic instability caused by the alteration of fluid properties due to bacterial metabolic activity, we tested the effect of displacing the suspending fluid with the supernatant. We prepared a bacterial suspension with a volume fraction of $\phi_0 \approx 0.825\%$ and left the suspension undisturbed for three hours, after which we filtered the suspension to remove the bacteria. The fluid collected (supernatant) was then used to carry out the displacement experiment. We observed no emergence of instability in the front, indicating that any changes in the suspending fluid characteristics due to bacterial metabolic activity do not contribute to the instability observed.

To determine whether the threshold ϕ_c for the onset of instability varied with geometry, we conducted experiments using the QFS geometry set-up. Again, experiments carried out at a very low bacterial volume fraction (Fig. 2(i)) showed fields propagating similar to that of two Newtonian fluids with no viscosity contrast displacing each other(Movie3). However, for $\phi_0 \approx 0.825\%$, the fields first showed multiple fingers, which appeared in the divergent part of the cell; these fingers then merged and flowed towards the outlet (Figs. 2(g) and 2(h)) Movie4). Fig. 3(a) shows the volume fraction profiles of the four different regimes identified in Fig. 1(b): at very low bacterial volume fraction, the profile exhibited a smooth and error-function-like pattern (red line: diffusive regime). At high bacterial volume fraction, a sharp shock front was observed (green line: finger regime) similar to that observed in viscous fingering experiments [51–53]. In addition to these two regimes, we pointed out the rounded regime (yellow line) and the spike regime (purple line), where the latter is characterized by a spike of low bacterial volume fraction which traveled ahead of the front.

In the finger regime, a shock front is visible at all times (Fig. 3(b)) and corresponds to a iso volume fraction range of $0 \lesssim \phi/\phi_0 \lesssim 0.5$. Fig. 3(c) shows the temporal variation of three iso volume fraction positions. We observe that these positions $y(\frac{\phi}{\phi_0})$ vary linearly with time. The green symbols in Fig. 3(d) show the normalized velocities $V(\frac{\phi}{\phi_0})/U$ obtained from the slopes of $y(\frac{\phi}{\phi_0})$ as a function of time. The region of volume fractions that corresponds to the sharp shock front ($0 \lesssim \frac{\phi}{\phi_0} \lesssim 0.5$) propagates at a normalized velocity ~ 1.4 faster than the average velocity of the fluid in a self-similar way. When ϕ_0 decreases to $\approx 0.55\%$ (▷ in Fig. 3(d)), the constant velocity plateau (the shock) disappeared. It is replaced by (i) a rapid drop of $V(\phi/\phi_0)/U$ for $\phi/\phi_0 \lesssim 0.15$ and (ii) a slower decrease for $\phi/\phi_0 \gtrsim 0.15$ towards ~ 1. The first sharp drop comes from a spike that contains a small number of bacteria that propagates ahead of the front. When ϕ_0 decreases further to $\approx 0.33\%$ (□ in Fig. 3(d)), the spike disappears, and every iso-ϕ's of the profile spread in time

with a $V(\phi/\phi_0)/U$ that decreases monotonically towards 1 when $\phi/\phi_0 \to 1$. This is the rounded regime. Finally, in the diffusive regime, for ϕ_0 down to $\approx 0.11\%$ (◯ in Fig. 3(d)), all the iso-ϕ's lines travel at a constant velocity close to ~ 1. These features are identical to those observed when a less viscous fluid displaces a more viscous fluid [38, 51–53] and, the volume fraction of bacteria ϕ_0 seems to play a similar role to that of the viscosity ratio M for Newtonian fluids.

To test this idea, we characterized the shape of the front by its width λ (SI III) and its dynamics by the tip velocity V_f, as functions of ϕ_0/ϕ_c. The □ in Fig. 4(a) illustrate the variation of the finger width λ normalized by the channel width W. For $\phi_0 \lesssim \phi_c$, the normalized finger width is close to 1, and the instability is absent. The normalized width decreases rapidly for $\phi \gtrsim \phi_c$ and tends towards half of the cell's width, emphasizing the emergence of fingers. To support this observation, experiments were conducted using bacterial suspensions of different critical volume fractions ϕ_c. In MB, for instance, the bacteria swim at a slower speed ($V_s = 10.6 \pm 1.2$ μm.s^{-1}), and the rotational diffusion coefficient is higher ($D_R = 0.13 \pm 0.02$ s^{-1}) compared to MB+1% PVP. As a result, a larger quantity of bacteria $\phi_c \approx 0.99\%$ is needed to reach the zero viscosity regime. ◯ in Fig. 4(a) shows the value of λ/W as a function of ϕ_0/ϕ_c for a suspension of bacteria in MB displacing MB. We observed again that λ/W decreases to ~ 0.5 for $\phi \gtrsim \phi_c$, which corresponds to the fingering instability emergence. In the same way, we observe that at low ϕ_0, the normalized tip velocities are close to 1 (Fig. 4(b)), and fingers are absent. The same analyses were conducted on experiments with Newtonian fluid pairs. The results shown in SI IV indicate that when the viscosity contrast is approximately 3, the displacement front becomes unstable [43, 52]. Referring to Fig. 1(c), we observe that the normalized volume fraction ϕ_0/ϕ_c needed to achieve this viscosity ratio is approximately 0.5. Experiments conducted with this volume fraction demonstrate a stable front, which is equal in width to that of the cell (Fig. 4(a)), moving at the average velocity of the fluid (Fig. 4(b)). This indicated that the instability observed with bacterial suspensions is specific to a threshold linked to the zero-viscosity regime. It emphasizes the importance of using a suspension with a volume fraction greater than ϕ_c to observe the emergence of an instability.

Another difference with Newtonian fluids is that in the unstable configuration, increasing the flow velocity leads to the formation of multiple fingers [39, 53–55]. Surprisingly, with bacteria, we observed the finger regime to disappear when the velocity was increased to 100 μm.s^{-1}. One way to explain this is through the unique rheological behavior of the bacterial suspensions [21–23]. At low shear rates, the suspensions show a low-viscosity Newtonian plateau, whose value (represented by ◊ in Fig. 1(c)) changes with the bacterial volume fraction. When the shear rates are higher than $\dot{\gamma}_c$, the suspensions exhibit a second higher Newtonian plateau with a viscosity close to that of the suspending fluid (represented by ◯ in Fig. 1(c)). The crossover between the two plateaus occurs for $\dot{\gamma}_c \sim 4D_R \sim 0.4$ s^{-1} [23]. If we assume a parabolic velocity profile in the aperture of the HS cell, the flow can be characterized by an average shear rate $\langle\dot{\gamma}\rangle = \frac{4U}{H}$. For velocities below 37 μm.s^{-1}, $\langle\dot{\gamma}\rangle$ is less than 0.4 s^{-1} *i.e.* below $\dot{\gamma}_c$. The fluid dynamics within the HS cell are affected by viscosity reduction, resulting in an effective low-viscosity fluid and the formation of a finger. For $U \sim 100$ μm.s^{-1}, $\langle\dot{\gamma}\rangle$ is ~ 1 s^{-1} higher than $\dot{\gamma}_c$ which leads to the second Newtonian plateau. The difference in viscosity between the displaced and injected fluids is then not enough to cause instability.

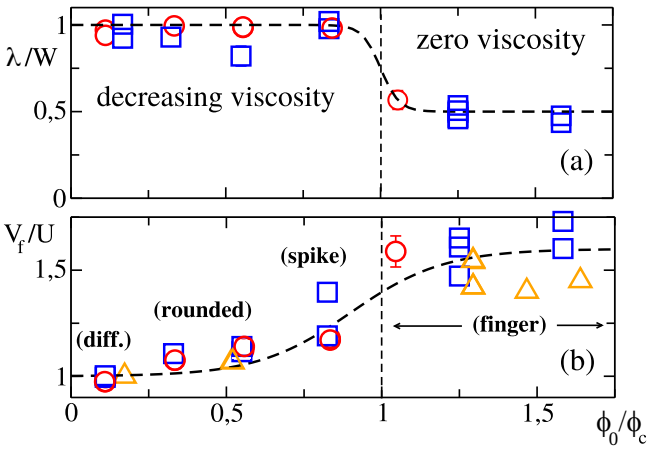

FIG. 4. Normalized finger width λ (a) and tip velocity V_f (b) as a function of the bacterial volume fraction ϕ_0 normalized with the critical volume fraction ϕ_c. □ and △: Bacteria in MB+1% PVP. ◯: Bacteria in MB. △: QFS experiments. □ and ◯: experiments in HS. Dotted line, adjustment by: $\sim tanh(\frac{\phi_0}{\phi_c} - 1)$. For the HS cell, $V_f = V(\phi/\phi_0 = 0.2)$ and U is $\simeq 17$ or 37 μm.s^{-1}. For the QFS experiments, V_f is the distance between the input and the output, normalized by the time taken to reach the output. In this case, $U \simeq 10$ μm.s^{-1}.

Discussion and conclusions.- We observed that introducing swimming bacteria into a flowing fluid can destabilize the interface between the bacterial front and the displaced fluid, resulting in a new interfacial dynamics. This instability was observed when both $\phi_0 \gtrsim \phi_c$ and $\langle\dot{\gamma}\rangle \lesssim \dot{\gamma}_c$ for which the bacterial suspension effective viscosity is zero. For lower ϕ_0, the swimming activity of the bacteria seems too weak to cause any such instability but leads to some alterations of the density profile. Another interesting observation is the emergence of vorticity in our experiments in a QFS geometry, which may be related to collective motion in the suspension. This observation supports the finding of a sudden increase in the length of velocity correlations, which reaches dimen-

sions comparable to the cell opening when $\phi_0 > \phi_c$ [22]. Future research may go beyond correlation to show their connection. We think our findings are crucial in situations where bacteria travel through tight spaces such as pores, fractures, or slits. They can

be useful for developing technology based on biology where reducing fluid viscosity is important, for example, in microbial-enhanced oil recovery (MEOR).
By showing that activity at the individual particle's scale can control the fluid's effective property and influence fluid flow, our results also significantly contribute to the already rich field of active matter and open new paths for further research.

Acknowledgements We thank A. Gargasson, A. Aubertin, C. Manquest, L. Auffray, and R. Pidoux for experimental help, and H. Stone, F. Moisy, M. Jarrahi, G. Dietze and F. Doumenc for fruitful discussions. This work is supported by the French National Research Agency (ANR) through the "Laboratoire d'Excellence Physics Atom Light Mater" (LabEx PALM) as part of the "Investissements d'Avenir" program (ANR-10-LABX-0039). H.A. acknowledged the support of CNRS 80 | PRIME through the project RootBac.

* harold.auradou@universite-paris-saclay.fr

[1] E. Lauga and T. R. Powers, Reports on Progress in Physics, **72**(9):096601 (2009).
[2] K. Drescher, J. Dunkel, L. H. Cisneros, S. Ganguly, and R. E. Goldstein, Proceedings of the National Academy of Sciences, **108**(27):10940–10945 (2011).
[3] A. Sokolov and I. S. Aranson, Physical Review Letters, **109**:248109 (2012).
[4] A. Rabani, G. Ariel and A. Be'er, PLoS ONE, **8**(12):e83760 (2013).
[5] E. Lushi, H. Wioland, and R. E. Goldstein, Proceedings of the National Academy of Sciences, **111**(27):9733–9738 (2014).
[6] J. Gachelin, A. Rousselet, A. Lindner, and E. Clément, New Journal of Physics, **16**(2):025003 (2014).
[7] H. Wioland, F. G. Woodhouse, J. Dunkel, J. O. Kessler, and R. E. Goldstein, Physical Review Letters, **110**:268102 (2013).
[8] D. Nishiguchi, I. S. Aranson, A. Snezhko, and A. Sokolov, Nature Communications, **9**(11):4486 (2018).
[9] R. Rusconi, J. S. Guasto, and R. Stocker, Nature Physics,**10**(3):212–217 (2014).
[10] L. Vennamneni, S. Nambiar, and G. Subramanian, Journal of Fluid Mechanics, **890**:A15 (2020).
[11] B. Ezhilan and D. Saintillan, Journal of Fluid Mechanics, **777**:482–522 (2015).
[12] A. Ganesh, C. Douarche, M. Dentz, and H. Auradou, Phys. Rev. Fluids, **8**:034501 (2023).
[13] X.-L. Wu and A. Libchaber, Physical Review Letters, **84**(13):3017–3020 (2000).
[14] R. Di Leonardo, L. Angelani, D. Dell'Arciprete, G. Ruocco, V. Iebba, S. Schippa, M. P. Conte, F. Mecarini, F. De Angelis, and E. Di Fabrizio, Proceedings of the National Academy of Sciences, **107**(21):9541–9545 (2010).
[15] A. Sokolov, M. M. Apodaca, B. A. Grzybowski, and I. S. Aranson, Proceedings of the National Academy of Sciences, **107**(3):969–974 (2010).
[16] A. Ganesh Hal sciences (Thesis: tel-03999273), Université Paris-Saclay (2023).
[17] J. Bouvard, F. Moisy, and H. Auradou, Physical Review E, **107**(4):044607 (2023).
[18] S. Ramaswamy, Annual Review of Condensed Matter Physics,**1**(1):323–345 (2010).
[19] M. C. Marchetti, J. F. Joanny, S. Ramaswamy, T. B. Liverpool, J. Prost, Madan Rao, and R. Aditi Simha, Reviews of Modern Physics, **85**(3):1143–1189 (2013).
[20] S. Ramaswamy, Journal of Statistical Mechanics: Theory and Experiment,**2017**(5):054002 (2017).
[21] H. M. López, J. Gachelin, C. Douarche, H. Auradou and E. Clément, Physical Review Letters, **115**(2):028301 (2015).
[22] V. A. Martinez, E. Clément, J. Arlt, C. Douarche, A. Dawson, J. Schwarz-Linek, A. K. Creppy, V. Škultéty, A. N. Morozov, H. Auradou, and W. C K Poon, Proceedings of the National Academy of Sciences, **117**(5):2326–2331 (2020).
[23] J. Y. Y. Chui, C. Douarche, H. Auradou, and R. Juanes, Soft Matter, **17**(29):7004–7013 (2021).
[24] Y. Hatwalne, S. Ramaswamy, M Rao, and R. Aditi Simha, Physical Review Letters, **92**(11) (2004).
[25] A. Sokolov and I. S. Aranson, Physical Review Letters, **103**(14) (2009).
[26] D. Saintillan, Experimental Mechanics, **50**(9):1275–1281 (2010).
[27] D. Saintillan, Physical Review E, **81**(5):056307 (2010).
[28] J. Gachelin, G. Miño, H. Berthet, A. Lindner, A. Rousselet and E. Clément, Physical Review Letters, **110**(26):268103 (2013).
[29] E. Clément, A. Lindner, C. Douarche, and H. Auradou. The European Physical Journal Special Topics, **225**(11-12):2389–2406 (2016).
[30] D. Saintillan, Annual Review of Fluid Mechanics, **50**(1):563–592 (2018).
[31] Z. Liu, K. Zhang, and X. Cheng, Rheologica Acta, **58**, 439–451 (2019).
[32] A. Choudhary, S. Nambiar, and H. Stark, Communications Physics, **6**(11):1–11 (2023).
[33] S. Hill, Chemical Engineering Science, **1**(6):247–253 (1952).
[34] P. G. Saffman and G. I. Taylor, Proceedings of Royal Society, **245**(1242):312–329 (1958).
[35] P. G. Saffman, Journal of Fluid Mechanics, **173**:73 – 94 (1986).
[36] W. B. Zimmerman and G. M. Homsy, Physics of Fluids A, **4**(11):2348–2359 (1992).
[37] J.-D. Chen, Journal of Fluid Mechanics, **201**(1):223 (1989).
[38] P. Petitjeans and T. Maxworthy, Journal of Fluid Mechanics, **326**:37-56 (1996).
[39] P. Tabeling and A. Libchaber. Physical Review A, **33**(1):794–796 (1986).
[40] P. Tabeling, G. Zocchi, and A. Libchaber, Journal of Fluid Mechanics, **177**:67–82 (1987).
[41] D. Bensimon, L. P. Kadanoff, S. Liang, B. I. Shraiman, and C. Tang, Reviews of Modern Physics, **58**(4):977–999

(1986).
[42] H. Thomé, M. Rabaud, V. Hakim, and Y. Couder, Physics of Fluids A: Fluid Dynamics, **1**(2):224–240 (1989).
[43] E. Lajeunesse, J. Martin, N. Rakotomalala, and D. Salin, Physical Review Letters, **79**(26):5254–5257 (1997).
[44] P. Petitjeans, C.-Y. Chen, E. Meiburg, and T. Maxworthy, Physics of Fluids, **11**(7):1705–1716 (1999).
[45] T. E. Videbæk, Physical Review Fluids, **5**(12):123901 (2020).
[46] D. Keable, A. Jones, S. Krevor, A. Muggeridge, and S. J. Jackson, Transport in Porous Media, **143** (1):23–45 (2022).
[47] P. Tabeling, G. Zocchi, and A.Libchaber, Journal of Fluid Mechanics, **177**:67-82 (1986).
[48] K. Baumgarten and B. P. Tighe, Soft Matter, **13**(45):8368–8378 (2017).
[49] N. Rakotomalala, D. Salin, and P. Watzky, Journal of Fluid Mechanics, **338**:277–297 (1997).
[50] C.-Y. Chen and E. Meiburg, Journal of Fluid Mechanics, **371**:233–268 (1998).
[51] E. Lajeunesse, J. Martin, N. Rakotomalala, D. Salin, and Y. C. Yortsos, Journal of Fluid Mechanics, **398**:299–319 (1999).
[52] I. Bischofberger, R. Ramachandran, and S. R. Nagel, Nature Communications, **5**(1):5265 (2014).
[53] I. Bischofberger, R. Ramachandran, and S. R. Nagel, Soft Matter, **11**(37):7428–7432 (2015).
[54] G. I. Taylor, Journal of Fluid Mechanics, **10**(2):161–165 (1961).
[55] S. Malhotra, M. M. Sharma, and E. R. Lehman, Physics of Fluids, **27**(1):014105 (2015).
[56] A. Einstein, Annalen der Physik, **324**(2):289–306 (1906).

Supplementary information

I Bacteria preparation

We used an Escherichia coli strain (RP437-YFP), a bacteria expressing yellow fluorescence protein. The growth medium consisted in a M9 minimal medium supplemented with 0.1% Casammino acids, 0.4% Glucose, 0.01% 1 M Calcium chloride and 0.2%, 1M Magnesium sulfate dissolved in milliQ water. To this growth medium, 25 μg/mL Chloramphenicol (CAM) was added to grow only the bacteria expressing yellow fluorescence preferentially. The bacteria were cultured in an incubator shaker at 240 rpm and 30°C. The culture was stopped at an OD close to ~ 0.1 and washed twice by centrifugation (2300 g for 10 min). The bacteria were then re-suspended into a minimal buffer (0.1 M EDTA, 0.001 M Methionine, 1 M Sodium Lactate, and 0.1 M Phosphate buffer dissolved in milliQ water at pH = 7.0). This medium provided the salts needed for bacterial swimming but contained no nutrients for bacterial growth. The concentrated bacteria were then diluted to the target concentration.

II Bacteria Motility

We characterized the motility of the bacteria by two parameters: the average swimming velocity and the rotational diffusivity of the bacteria. To determine those values, a microfluidic chamber (Length=2 cm, Width= 1 cm and Height=250 μm) created by bonding PDMS onto glass was filled with a suspension of bacteria ($\phi_0 \approx 0.033\%$). The suspension was placed under the microscope and observed using a 10x objective lens with a YFP filter. Images were then recorded at ten frames per second with an exposure time of 50 ms using a 2×2 binning for 20 s every 30 min over a period of 2 to 4 hours. The sequence of images was taken halfway between the top and bottom surfaces. The field of view is 1.3×1.3 mm^2 with a depth ~ 30 μm. Bacterial tracks were computed from the sequences of phase fluorescent images using Trackmate and post processed using an in-house MATLAB code.

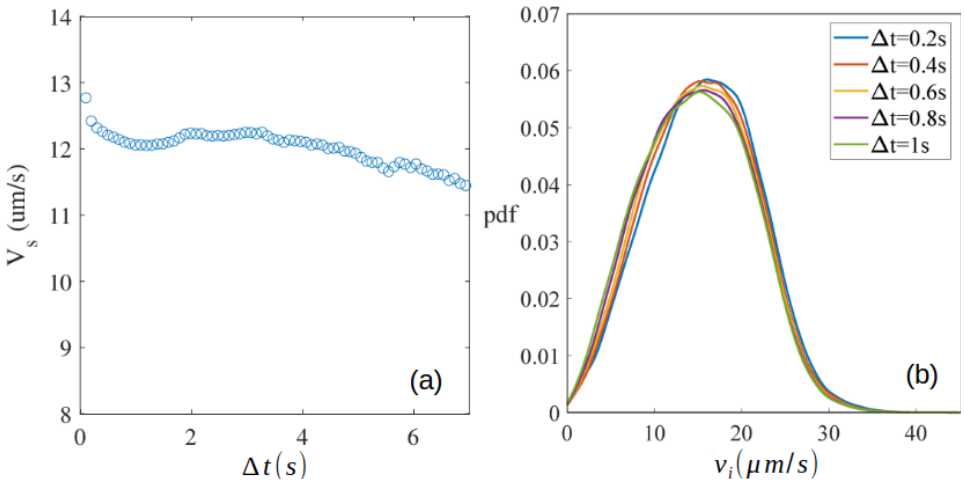

Figure 1: (a) Average velocity as function of the sampling time Δt. (b) Distribution of the velocities $||\mathbf{v}_i||$ for different sampling time Δt

For each track i, the two-dimensional positions $\mathbf{x}_i(t) = (x_i(t), y_i(t))$ was used to compute the two-dimensional velocities $\mathbf{v}_i(t) = \Delta\mathbf{x}_i/\Delta t$ using a sampling time Δt. Fig. 1a shows the average velocity determined from one of the image sequences as a function of the sampling time Δt. The average velocity varied weakly with Δt and was almost constant for Δt between $\simeq 0.5$ and $\simeq 4$ seconds. This weak dependence was confirmed by the fact that the velocity distributions plotted for different Δt were superimposed (See Fig. 1b). The values of V_s were obtained using $\Delta t = 0.4s$.

To determine the rotational diffusivity of the bacteria, the dot product of the velocity vector projections $\mathbf{v}_i(t).\mathbf{v}_i(t+\tau)$ were calculated for different time intervals τ. The magnitude of velocities then normalized the values averaged over time and tracks to obtain the mean cosine angle of projection between these two vector projections $cos\theta(\tau)$.

$$cos\,(\theta(\tau)) = \langle \frac{\mathbf{v}_i(t).\mathbf{v}_i(t+\tau)}{||\mathbf{v_i(t)}||||\mathbf{v_i(t+\tau)}||} \rangle_{i,t} \tag{1}$$

In Fig. 2, we observe two relaxation time scales: a first rapid drop followed by another drop with a smaller slope for $\tau > 0.7$s. The first slope was attributed to the noise and the second to the rotational diffusivity D_R due to the bacteria's run-and-tumble motion. To estimate D_R, we fitted the curve with an exponentially decaying function from $\tau = 1.5$ to 10 s using

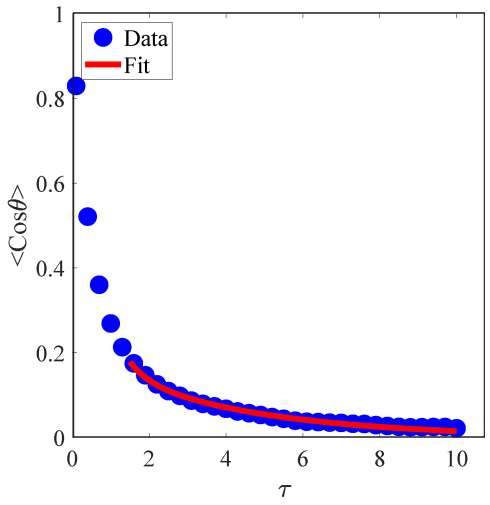

Figure 2: $cos\,(\theta(\tau))$ plotted as function of τ for $\phi_0 = 0.33$ suspended in MB. The solid line is the fit of the data with $cos\,(\theta(\tau)) = Ae^{-2D_R\tau}$.

$cos\,(\theta(\tau)) = Ae^{-2D_R\tau}$ [1].

III Method used to determine the finger width

The following section outlines how the width of digitations were determined. The process begins with the volume fraction fields $\phi(x, y)$. Examples of fields are shown in Fig.2 in the main paper. First, the iso-volume fraction line $\frac{\phi(x,y)}{\phi_0}$=0.6 is extracted using a in-house MATLAB code. Fig. 3 showcases examples of iso-volume fraction lines in the case of experiments performed with bacteria and iso concentration lines for experiments performed with fluorescein obtained for various experiments where we injected the same fluid volume. The difference in viscosity or the concentration of bacteria can have a significant impact on the part of the front that advances in the fluid initially placed in the Hele–Shaw cell, as demonstrated in the figure.

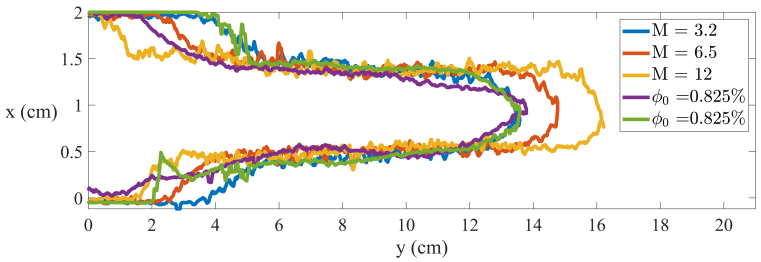

Figure 3: Iso line $\phi/\phi_0 = 0.6$ for experiments performed in a channel of width W=2 cm. The blue, red, and yellow curves are, respectively, for the Newtonian pairs of fluids for $M \simeq 3.2$, 6.5, and 12. The purple and green curves correspond to two repetitions of an experiment with a bacterial volume fraction $\phi_0 \approx 0.825\%$.

To characterize the width λ of the finger, we estimated the distance along x (transverse to the flow) separating the iso-concentration lines at a given position y (See Fig. 4a). Close to the inlet (See Fig. 4b), $\lambda(y)$ is approximately 2 cm, which is equal to the channel width. This zone is followed by a decrease in $\lambda(y)$ as we increase y. Then, $\lambda(y)$ is observed to reach an almost constant value along y. This asymptotic value of $\lambda(y)$ is about half the channel width. Finally, as we progress further and increase y, we observe $\lambda(y)$ decreasing again, corresponding to the region near the tip of the concentration front. The length of the finger, denoted as l, is defined as the distance between the positions in the y-axis where $\lambda(y) = 0$ and 2 cm as shown in Fig. 4a and b. We then average $\lambda(y)$ along length l to obtain λ.

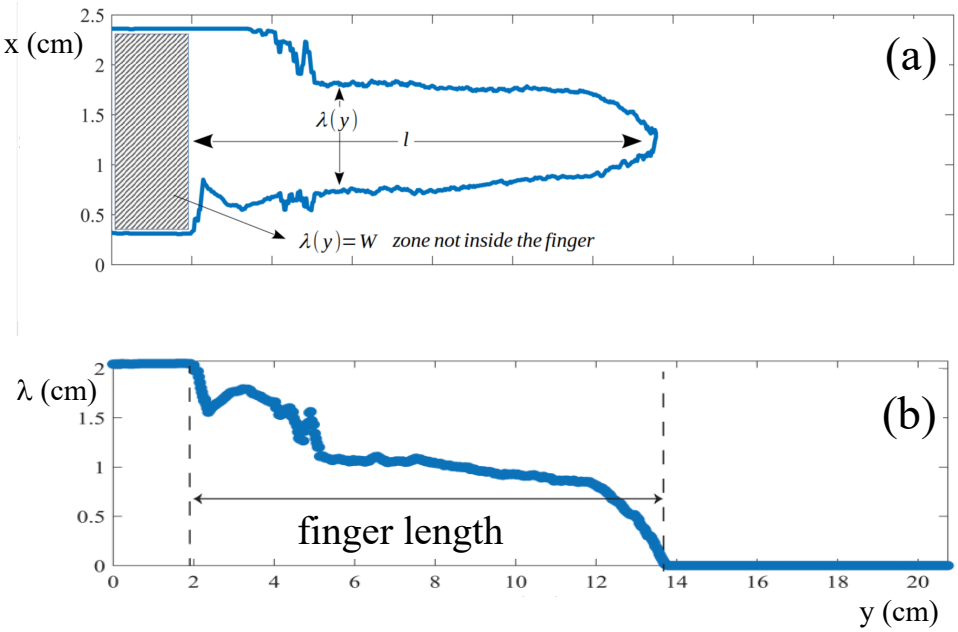

Figure 4: (a) Iso volume fraction line $\phi/\phi_0 = 0.6$ and (b) finger width $\lambda(y)$ obtained from the analysis of the iso volume fraction line. The line was obtained from a volume fraction field measured for an experiment performed with a bacterial volume fraction $\phi_0 \simeq 0.825\%$.

IV Characteristics of the profiles obtained with Newtonian fluids

The characteristics of the fronts created using Newtonian fluid pairs were also determined by applying the same methods as those used for the fronts measured with bacterial suspensions while moving the same fluid that contained no bacteria.

Fig. 5 shows the profiles obtained for three different pair of Newtonian fluids. The representation is identical to Fig. 3b of the paper. Note that all profiles have a shock at the front of the forehead, identified by an abrupt variation in concentration at the front.

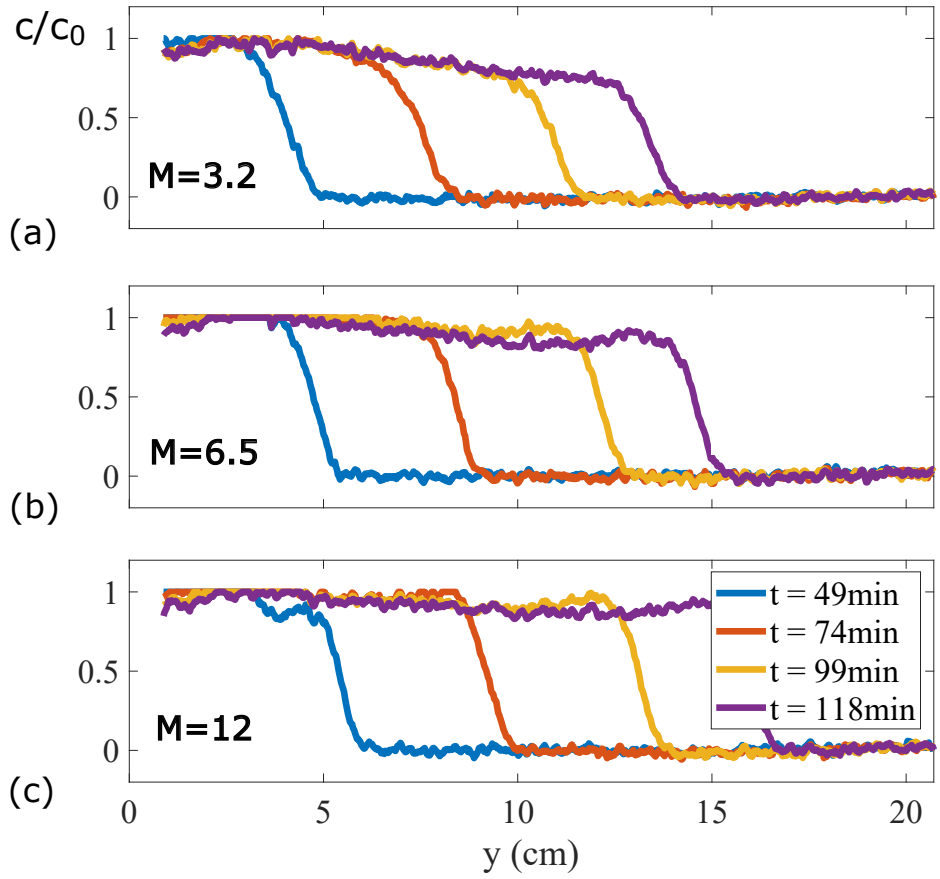

Figure 5: Normalized fluorescein concentration c/c_0 profiles measured in an HS cell of width $W = 2\ cm$ plotted as a function of the distance y, along the length of the cell. The experiments were realized with $c_0 = 0.02\ g/L$ and at a flow velocity $U = 17.5\ \mu m.s^{-1}$. The viscosity contrast between the displaced fluid (with viscosity μ_1) and the displacing fluid (with viscosity μ_2) was adjusted by adding PVP to the displaced fluid. (a) M=3.2 (Water dyed with florescein displaces 1% PVP solution), (b) M=6.5 (Water dyed with florescein displaces 2% PVP solution) and (c) M=12 (Water dyed with florescein displaces 3% PVP solution).

In our experiments with bacterial suspensions (refer to the main text), we determined the width of the fingers, denoted as λ, using the method outlined in SI III. Additionally, we measured the tip velocity, V_f, following

the definition provided in the body of the article. The variation of these two quantities is illustrated in Fig. 6. These data confirm that with a viscosity contrast of M=3.2, the front is unstable and characterized by digitation, which is half the width of the cell.

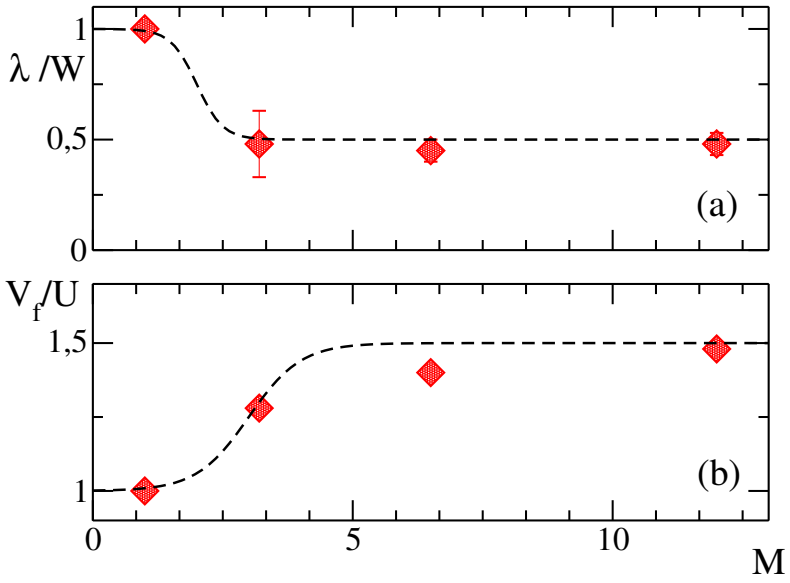

Figure 6: Normalized front finger width normalized by the channel width λ/W (a) and normalized tip velocity V_f/U as a function of the viscosity ratio $M = \mu_1/\mu_2$ between the displaced fluid (with viscosity μ_1) and the displacing fluid (with viscosity μ_2) was adjusted by adding PVP to the displaced fluid. Dotted line: adjustment by $\sim tanh(M - M_c)$ where $M_c = 2 \pm 1$ is the critical viscosity ratio.

References

[1] Jonathan Saragosti, Pascal Silberzan, and Axel Buguin. "Modeling E. coli Tumbles by Rotational Diffusion. Implications for Chemotaxis". In: *PLoS ONE* 7 ([**2012**]).